Science Advances
AAAS

Supplementary Materials for

Characterization of photoinduced normal state through charge density wave in superconducting $YBa_2Cu_3O_{6.67}$

Hoyoung Jang, Sanghoon Song, Takumi Kihara, Yijin Liu, Sang-Jun Lee, Sang-Youn Park, Minseok Kim, Hyeong-Do Kim, Giacomo Coslovich, Suguru Nakata, Yuya Kubota, Ichiro Inoue, Kenji Tamasaku, Makina Yabashi, Heemin Lee, Changyong Song, Hiroyuki Nojiri, Bernhard Keimer, Chi-Chang Kao, Jun-Sik Lee*

*Corresponding author. Email: jslee@slac.stanford.edu

Published 9 February 2022, *Sci. Adv.* **8**, eabk0832 (2022)
DOI: 10.1126/sciadv.abk0832

This PDF file includes:

Supplementary Text:

- RSXS measurement: The RSXS measurements were carried out at beamline 13-3 of the Stanford Synchrotron Radiation Lightsource (SSRL). The sample was mounted on an in-vacuum 4-circle diffractometer. The sample temperature was controlled by an open-circle helium cryostat. The x-ray was linearly and vertically polarized (σ-polarization), and the photon energy was tuned around Cu L_3-edge (932 eV). The exact (0, k, l) scattering plane was aligned by the measured (0, 0, 2), (0, −1, 1), and (1, 0, 1) structural Bragg reflections at the photon energy ~1770 eV. The scattering signal was obtained by a GaAs photodiode and normalized by the drain current on Au mesh.

- Analysis of transient behavior of the CDW intensity: To analyze the transient behavior of the CDW intensity on this YBCO cuprate after the optical pump, we first consider when the CDW peaks are changing. According to the CDW works in YBCO [12-14], there are three components to explain how the CDW peaks are changing: 1) Direct perturbation of Cu-charge state (e.g., photo-excited carrier); 2) Sample temperature change (heating); and 3) The known competing effect with SC (only at $T < T_c$ case). These components are respectively represented as blue-, red-, and purple-line in each panel, and the black-colored solid line shows their all summation. Note that each component consists of two exponential functions – decay and recovery with sample amplitude.

For the $T \geq T_c$ case, the temporal intensity change can be analyzed by components 1) and 2), except component 3). It is because the SC effect is not developed. In this case, as shown in Fig. S6a, the CDW firstly undergoes a fast melt near $\Delta t \sim 0$, and then the melted intensity recovers within a few ps time scales. This behavior is mainly explained by component 1). As the fluence increases, we found that the heat effect becomes pronounced with a longer time to recover to initial intensity.

Figure S6b shows an analysis of the temporal CDW intensity change under the superconducting state (i.e., $T < T_c$). It gets somewhat complicated because of the additional SC-related term (i.e., component 3). However, in this case, we could adapt the fitting parameters of components 1) and 2) analyzed at $T \geq T_c$ if the same fluence is used. For $T < T_c$, the overall temporal CDW intensity shows an enhancement because the SC becomes suppressed (Fig. 2). Similar to the case at $T = T_c$ (see Fig. S6a), the higher fluence induces more heat effect and slower the CDW intensity returning. Interestingly, the intensity maximized Δt becomes delayed as the fluence increases, i.e., from ~1 ps with 15 μJ/cm^2 to ~3 ps with 60 μJ/cm^2. We analyze this also comes from the pronounced heat effect in the higher fluence range. In order to minimize the heat effect during this study, we employed a mild pump fluence ~15 μJ/cm^2 in the tr-RSXS measurements.

- X-ray and optical pump penetration depth: According to CXRO database (The Center for X-Ray Optics at Lawrence Berkeley National Laboratory, https://www.cxro.lbl.gov/), the normal incidence penetration depth around Cu L_3-edge is estimated to be about 120 nm. Considering the sample angle ($\theta = 46°$ for $L = 1.46$) and the detector angle ($2\theta = 167°$), the RSXS probing depth is estimated as ~46 nm from the sample surface. According to the previous reports Refs. [35 (L. Stojchevska *et al.*) and 44 (B. Liu *et al.*)], the penetration depth of 800-nm pump laser in $YBa_2Cu_3O_{6+x}$ is estimated as the range of 80-200 nm.

- X-ray polarization effect in L-dependence of tr-RSXS measurement: As shown in Fig. 2a, the incident x-ray polarization signal is the *pi*(π)-polarization. Since the CDW intensity is proportional to $\pi' \cdot \pi = \cos(2\theta)$, the intensity was rescaled by multiplying $1/\cos(2\theta)$ to compare the intensities in *L*-dependence.

- Optical laser polarization effect in tr-RSXS measurement: In this study, we applied the *p*-polarized optical pump laser (i.e., *p* // *bc*-plane). Since the *p*-polarized laser has both components along the parallel and orthogonal direction to the CuO_2 plane, a pumping effect in the CuO_2 plane via the *p*-polarization is effectively weaker than that via the *s*-polarization (*s* // *ab*-plane). As shown in Fig. S7, the optical laser polarization effects were explored. We confirmed that the *p*-polarization needs more fluence to generate the similar effect shown the *s*-polarization, especially while the fluence value is high. For the fluence = 15 $\mu J/cm^2$, which was mainly used in this study, we could find that the difference between two polarizations is minimized.

Supplementary Figures:

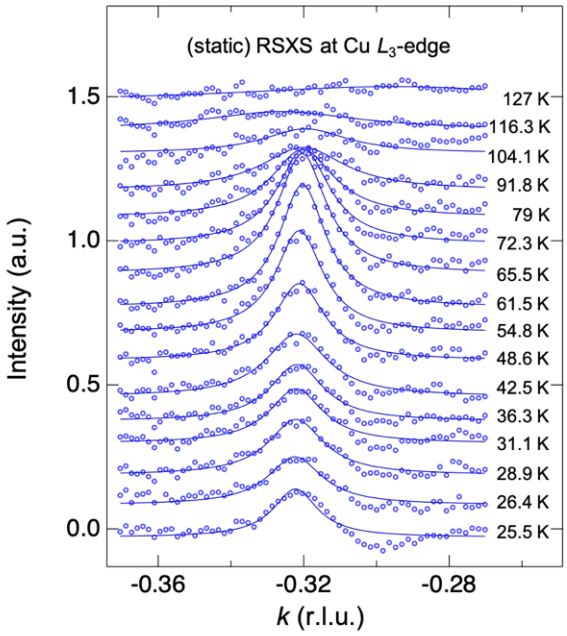

Fig. S1. Temperature dependence of the static CDW order in YBCO. The CDW peak observed at $\boldsymbol{Q}$ = (0, q_{cdw}, ~1.45) where q_{cdw} is around -0.32 reciprocal lattice unit (r.l.u.). The data are subtracted by high temperature (~150 K) data. Solid lines are Lorentzian fits to the data.

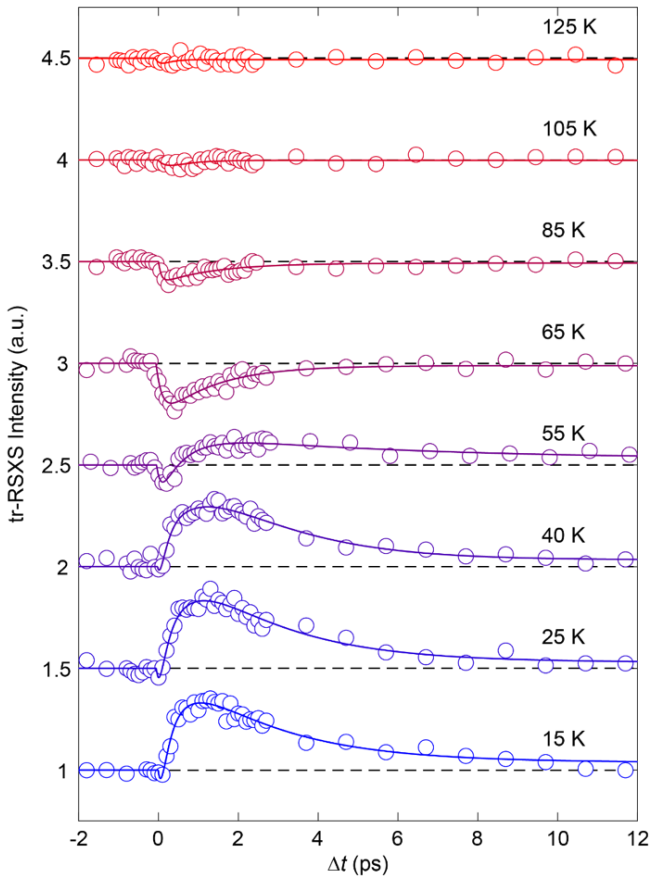

Fig. S2. Temporal behavior of the CDW order as a function of temperature. The tr-RSXS intensity was recorded at the CDW at $\boldsymbol{Q}$ = (0, -0.32, ~1.45). Each delay data has been vertically shifted for clarity. The solid line presents fitting by exponential functions. The dashed lines are baselines determined from the negative delay region.

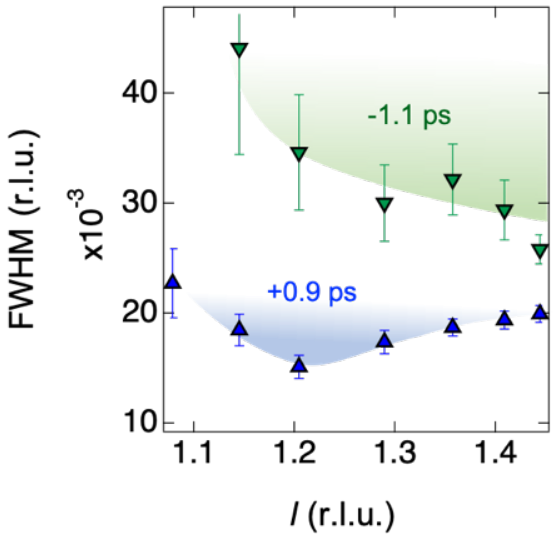

Fig. S3. *L*-dependence of photoinduced CDW. Fitted FWHM of the CDW peaks at l positions (i.e., 2θ) of Δt = +0.9 ps (up-triangles) and -1.1 ps (down-triangles). Blue and green colored shades are guides-to-the-eye. The error bars represent 1 standard deviation (s.d.) of the fit parameters.

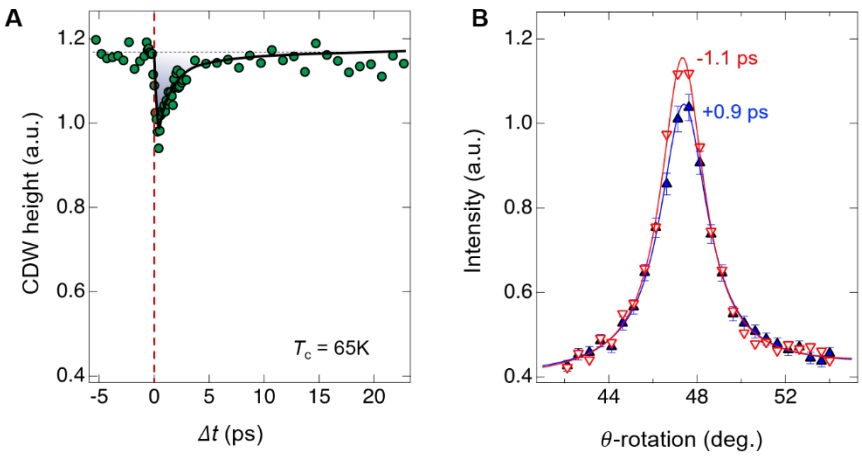

Fig. S4. Photoinduced CDW behavior. (**A**) CDW intensity at $\boldsymbol{Q}$ = (0, -0.32, 1.45) as a function of Δt, measured at T = 65 K (~ T_c). For $\Delta t < 0$, the data indicate the CDW intensity before the pump. For $0 < \Delta t <$ ~ 5 ps, the CDW is melted by the optical pump and then is recovered. The maximum melting of CDW occurs at Δt ~ 0.2 ps. The dashed lines are guides-to-the-eye. (**B**) The CDW peak profiles at Δt = -1.1 ps and Δt = +0.9 ps. At Δt = 0.9 ps, the CDW intensity recovered to about 83 % of the intensity at $\Delta t < 0$. Solid lines are Lorentzian fits to the data with a linear background.

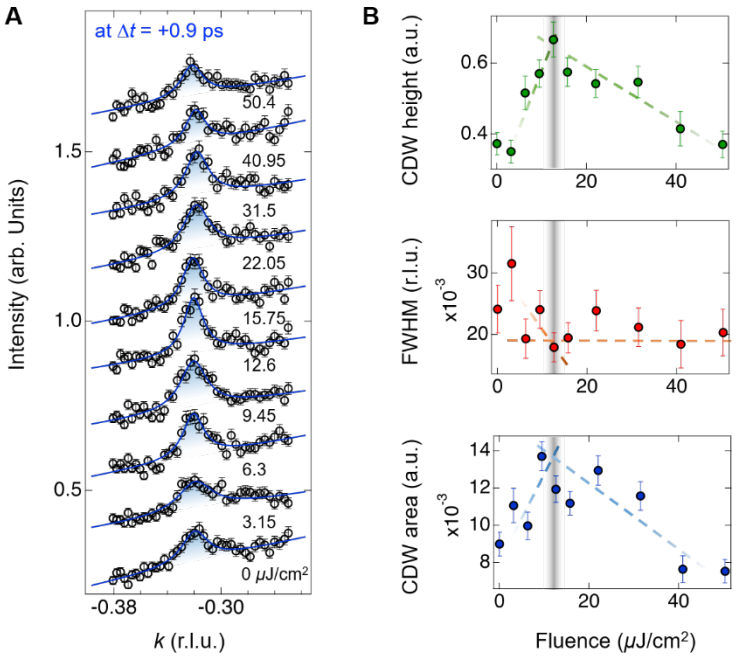

Fig. S5. Fluence dependence of photoinduced CDW.(**A**) CDW intensity at $\boldsymbol{Q}$ = (0, -0.32, 1.45) with varying laser fluence, measured at T = 25 K and Δt = +0.9 ps. The blue colored lines are Lorentzian fits to the data with a linear background. Each fluence data are vertically shifted by ~ 0.3 arb. Units. (**B**) Fitted CDW peaks with the different fluence – top: CDW peak's height, middle: FWHM, bottom: integrated intensity (CDW area). The error bars represent 1 standard deviation (s.d.) of the fit parameters. Gray colored shade denotes the employed fluence value in the tr-RSXS. All dashed lines are guides-to-the-eye.

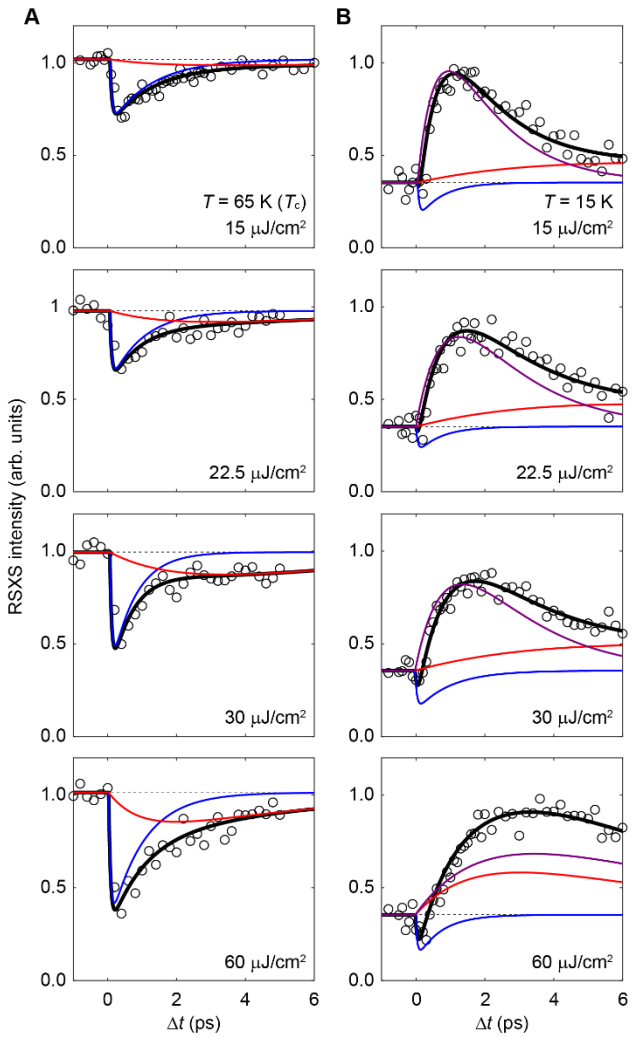

Fig. S6. Fluence-dependent delay scans of CDW. Data taken at (0, -0.32, 1.45) and at (**A**) 65 K (T_c), (**B**) 15 K. From top to bottom panels, incident fluence increases. Blue, red, and purple lines present fitting of direct perturbation, heating, and SC effect, respectively. Black solid lines show their summation. Black dashed lines display the intensity at $\Delta t < 0$.

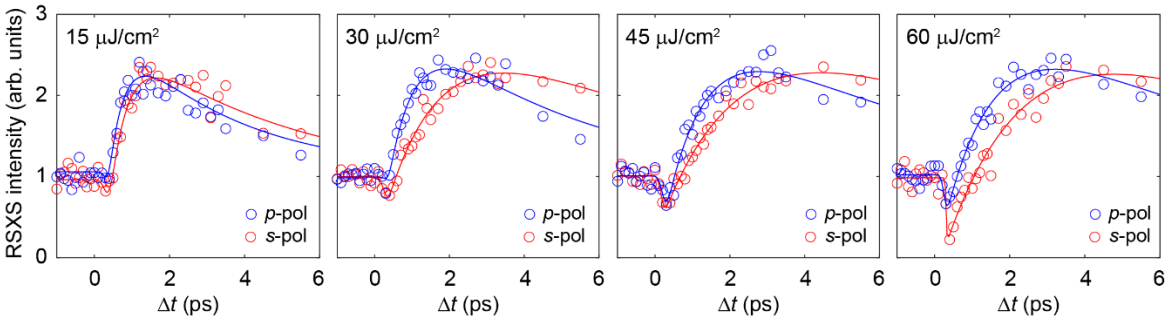

Fig. S7. Optical pump laser polarization effect of delay scans of CDW. Data taken at (0, -0.32, 1.45) and 20 K. *p*-pol (*s*-pol) is parallel to the crystalline *bc* (*ab*)-plane. The solid lines present exponential fitting.

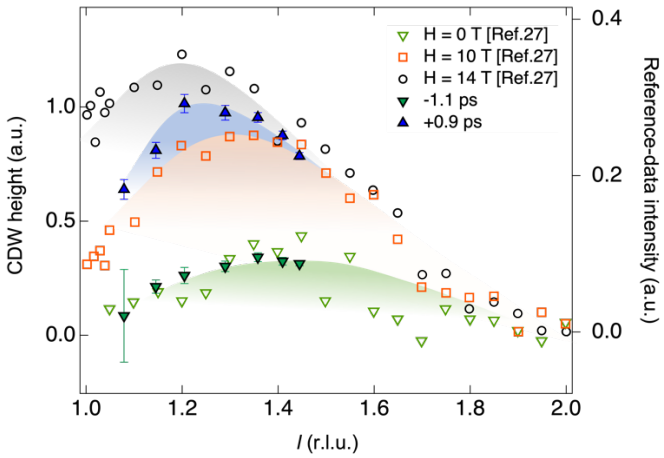

Fig. S8. Comparison of *L*-dependence between the pump-probe and the magnetic field. The magnetic data were taken from the Ref. [27] (Chang *et al.*). To superpose two different data set, we converted x-axis of the reference (x_{ref}) as follow: $l = 2 - x_{\mathrm{ref}}$. Also, it is important to note that the magnetic (H) field data in the reference were measured at $T = 22$ K (this study: $T = 25$ K). Also, the H-field study was measured by the non-resonant hard x-ray scattering (this study by resonant soft x-ray scattering).

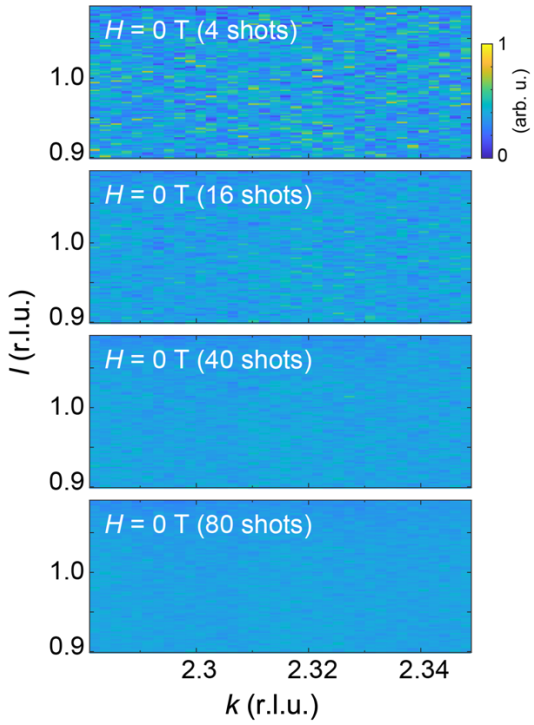

Fig. S9. Noise level comparison depending on the number of shots in the magnetic field experiment. All panels show *kl*-space around (0, 2+q_{cdw}, 1) under H = 0 T. The panels (from top to bottom) are 4-, 16-, 40-, and 80-shots average, respectively. With increasing the shot acquisition, the noise level is reduced.